Atmos. Chem. Phys. Discuss., 14, 28483–28522, 2014
www.atmos-chem-phys-discuss.net/14/28483/2014/
doi:10.5194/acpd-14-28483-2014

Atmospheric Chemistry and Physics Discussions

Stably stratified canopy flow in complex terrain

X. Xu[1,2], **C. Yi**[1], **and E. Kutter**[1,2]

[1]Queens College, City University of New York, Flushing, NY 11367, USA
[2]The Graduate Center, City University of New York, New York, NY 10016, USA

Received: 4 September 2014 – Accepted: 17 October 2014 – Published: 17 November 2014

Correspondence to: C. Yi (cyi@qc.cuny.edu)

Published by Copernicus Publications on behalf of the European Geosciences Union.

Abstract

The characteristics of stably stratified canopy flows in complex terrain are investigated by employing the Renormalized Group (RNG) k-ε turbulence model. In this two-dimensional simulation, we imposed persistent constant heat flux at ground surface and linearly increasing cooling rate in the upper canopy layer, vertically varying dissipative force from canopy drag elements, buoyancy forcing induced from thermal stratification and the hill terrain. These strong boundary effects keep nonlinearity in the two-dimensional Navier–Stokes equations high enough to generate turbulent behavior. The fundamental characteristics of nighttime canopy flow over complex terrain measured by a few multi-tower advection experiments can be produced by this numerical simulation, such as: (1) unstable layer in the canopy, (2) super-stable layer associated with flow decoupling in deep canopy and near the top of canopy, (3) upward momentum transfer in canopy, and (4) large buoyancy suppression and weak shear production in strong stability.

1 Introduction

Canopy flow occurring within and immediately above vegetation canopies plays a substantial role in regulating atmosphere–biosphere interaction. The canopy layer is an interface between land and atmosphere, in which most natural resources humans need are produced by biochemical reactions. Canopy flow influences those biochemical processes through the control of gas exchange between the vegetation and the atmosphere (e.g., influencing reaction rates by changing gas concentrations), heat exchanges (e.g., influencing reaction conditions by changing temperature), and momentum exchanges (e.g., changing turbulent mixing conditions). Better understanding of canopy flow behavior has many practical implications in accurately determining, for instance, terrestrial carbon sinks and sources (Sun et al., 2007), the fate of ozone within

ACPD
14, 28483–28522, 2014

and above forested environments (Wolf et al., 2011), forest fire spread rate (Cruz et al., 2005), bark beetle management (Edburg et al., 2010), and others.

The typical patterns of forest canopy turbulent flows are characterized by an S-shaped wind profile with an exponential Reynolds stress profile rather than the widely-used logarithmic wind profile and constant Reynolds stress observed over bare ground (Yi, 2008). S-shaped wind profiles have been observed within forest canopies in numerous studies (Baldocchi and Meyers, 1988; Bergen, 1971; Fons, 1940; Lalic and Mihailovic, 2002; Landsberg and James, 1971; Lemon et al., 1970; Meyers and Paw U, 1986; Oliver, 1971; Shaw, 1977; Turnipseed et al., 2003; Yi et al., 2005; Queck and Bernhofer, 2010; Sypka and Starzak, 2013). The S-shaped profile refers to a secondary wind maximum that is often observed within the trunk space of forests and a secondary minimum wind speed in the region of greatest foliage density. The features of S-shaped wind profiles imply that K-theory and mixing-length theory break down within a forest canopy layer (Denmead and Bradley, 1985; Yi, 2008). Particularly, the assumption of a constant mixing-length within a canopy is not consistent with the original mixing-length theory. This is because a mixing-length (l_m) must satisfy von Karman's rule (von Karman, 1930; Schlichting, 1960; Tennekes and Lumley, 1972), which indicates that a mixing length is a function of velocity distribution (Schlichting, 1960), as:

$$l_m = \kappa \left| \frac{dU/dz}{d^2U/dz^2} \right|$$

where κ is von Karman's constant, U is wind speed, and z is height within the canopy. The mixing length of the S-shaped velocity distribution is not constant, being minimum at the local extreme values of the wind profile ($dU/dz = 0$, $d^2U/dz^2 \neq 0$) and maximum at the inflection point of the wind profile ($dU/dz \neq 0$, $d^2U/dz^2 = 0$) (Wang and Yi, 2012). A mixing-length that varies with height within canopy has been demonstrated by large-eddy simulations (Coceal et al., 2006; Ross, 2008) and by water tank experiments (Poggi and Katul, 2007).

ACPD
14, 28483–28522, 2014

The features of S-shaped wind profiles also dictate the existence of super-stable layers near levels where wind speed is maximum (or minimum) and temperature inversion (temperature increasing with height) exists, leading the Richardson number to be extremely large or infinity (Yi et al., 2005). A super-stable layer acts as a "lid" or "barrier" that separates fluid into two uncorrelated layers: (1) the lower layer between the ground and the super-stable layer, and (2) the upper layer above the super-stable layer. This canopy flow separation was verified by SF_6 diffusion observations (Yi et al., 2005) and carbon isotope experiments (Schaeffer et al., 2008). The lower layer is sometimes called a "decoupled layer" (Alekseychik et al., 2013) that is shallow, usually within the trunk space of a forest. Because the super-stable layer prohibits vertical exchanges, the decoupled layer channels air in the horizontal direction. The characteristics of the channeled air are highly dependent on soil conditions, containing a high concentration of soil respired CO_2 and soil evaporated water vapor, and consisting of colder air cooled by radiative cooling at the ground surface (Schaeffer et al., 2008). The channeled air is sometimes termed "drainage flow", and is a common phenomenon in hilly terrains under stable atmospheric conditions, such as on calm and clear nights (Yi et al., 2005; Alekseychik et al., 2013). The drainage flow limits the accuracy of tower-based estimates of ecosystem-atmosphere exchanges of carbon, water, and energy. Sensors on the tower above the canopy cannot measure the fluxes conducted by drainage flow because the layer above the canopy is decoupled from the drainage flow by the isolating super-stable layer. This advection problem is a well-known issue that has not yet been solved using eddy-flux measurements (Goulden et al., 1996; Aubinet et al., 2003; Staebler and Fitzjarrald, 2004; Sun et al., 2007; Yi et al., 2008; Montagnani et al., 2009; Feigenwinter et al., 2010; Aubinet and Feigenwinter, 2010; Queck and Bernhofer, 2010; Tóta et al., 2012; Siebicke et al., 2012).

The concept of a super-stable layer is useful in interpreting data associated with stratified canopy air (Schaeffer et al., 2008). However, stratified canopy flows over complex terrain are far too complex to be able to characterize considering only a super-stable layer. Canopy structure (quantified by leaf area density profile), terrain slope, and ther-

ACPD
14, 28483–28522, 2014

mal stratification are three key parameters in understanding the details of stratified canopy flows over complex terrain. The thermal stratification plays a leading role in the development of pure sub-canopy drainage flows (Chen and Yi, 2012): strong thermal stratification favors drainage flow development on gentle slopes, while weak or near-neutral stratification favors drainage flow development on steep slopes. We speculate that interaction between thermal stratification and terrain slopes and vegetation canopy may result in multiple super-stable layers and complicated flow patterns, causing difficulties in understanding the mechanisms and rates of exchange of mass and energy between the terrestrial biosphere and the atmosphere (Alekseychik et al., 2013; Burn et al., 2011; Yi et al., 2005).

In this paper, we attempt to use a computational fluid dynamics (CFD) technique to examine the micro-structure of stratified canopy flows to provide insight into the role of physical processes that govern drainage motion and its turbulent characteristics within canopy in complex terrain. There are many challenges to face when pursuing this goal. First, the mixing-length theory and K-theory that are widely used as closure approaches to momentum equations (Wilson et al., 1998; Pinard and Wilson, 2001; Ross and Vosper, 2005; Katul et al., 2006) have been shown to have questionable validity within a forest canopy layer both theoretically (Yi, 2008) and observationally (Denmead and Bradley, 1985). Second, even though CFD models have been used to simulate flow within and above the canopy in numerous published studies, most numerically reproduced canopy flow is confined to idealized cases: either neutral (Ross and Vosper, 2005; Dupont et al., 2008; Ross, 2008; Katul et al., 2006) or weakly unstable (Wang, 2010) atmospheric conditions; or flat terrain with a homogeneous and extensive canopy (Huang et al., 2009; Dupont et al., 2010). Simulations of stratified canopy flow have received little consideration. This might be attributed to difficulties in numerical simulations arising from small scales of motion due to stratification (Basu et al., 2006), and complex interaction between wind and canopy drag elements (Graham and Meneveau, 2012). Large eddy simulation has been quite successful in producing turbulent flow and its related scalar transport in neutral and unstable cases (Shen and

ACPD
14, 28483–28522, 2014

Leclerc, 1997; Wang, 2010; Mao et al., 2008). However, under stably-stratificated conditions, computational cost of the LES-SGS models is incredibly increased due to the characteristic size of eddies is very small (Basu and Porté-Agel, 2006). If resolution is high enough, any turbulent flow can be simulated accurately by LES. In fact, given sufficiently fine resolution, LES becomes Direct Numerical Simulation (DNS), demanding very fine spatial and temporal resolution (Galperin and Orszag, 1993), which is currently beyond the reach of available computational power.

In this paper, we employ the renormalized group (RNG) k-ε turbulence model to investigate stably stratified canopy flows in complex terrain. The RNG k-ε turbulence model was developed by Yakhot and Orszag (1986a) using the renormalized group methods and prescribes the turbulent length scale related to transport of turbulent kinetic energy and dissipation rate (Yakhot and Orszag, 1986b; Smith and Reynolds, 1992). Compared to standard k-ε turbulence model, RNG k-ε turbulence model does not involve any experimentally adjustable parameters and has a rate of strain term in the dissipate transport equation, which is important for treatment of flows in rapid distortion limit, e.g. separated flows and stagnated flows (Biswas, and Eswaran, 2002) which commonly occur in vegetated hilly terrain. The initial successes in applying the RNG k-ε turbulence model to generate airflows in hilly terrain have been demonstrated by Kim and Patel (2000) and Xu and Yi (2013).

2 Method

2.1 Numerical implementation

The two dimensional computational domain extends over 1400 m × 130 m in a Cartesian coordinate system, corresponding to 1200 × 157 grid intervals in the x and y directions. A single hill is 100 m long covered with a 15 m tall homogeneous forest canopy, which extends from 650 m of the domain in horizontal. The mesh spacing in both horizontal and vertical at the forested hill is 0.5 m and is stretched with a power law, starting with

ACPD
14, 28483–28522, 2014

a grid spacing of 0.5 m throughout the canopy, with a larger grid spacing stretching outwards from the edge of the forest and the top of the canopy on the hill crest. The stretch power in both horizontal and vertical is 1.15. Ground surface roughness height is set to be 0.01 m.

In this study, the topography is specified with a ridge-like sinusoidal hill, infinite in the unsimulated third dimension. The shape function of the hill in 2-D is defined as

$$H(x) = \frac{H}{2}\cos\left(\frac{\pi x}{2L}\right) + \frac{H}{2} \quad (1)$$

where H is the hill height, L is the half length scale (half of the hill width at mid-slope height), x is longitudinal distance with $x = 0$ at the center of the single hill. The variation of the slope (H/L) is specified by changing H with a constant $L = 25$ m.

The porous canopy layer (canopy height $h = 15$ m) is designed horizontally homogeneous along the slope. Leaf area density profile $a(z)$ is specified as values from observation of an actual forest (Yi et al., 2005) with the maximum leaf area density at about 8 m. Leaf area index (LAI) is 3.3. The ambient temperature is $\theta_0(z) = \theta_{00} + \gamma z$, where $\theta_{00} = 288$ K, is the potential temperature at $z = 0$, γ is ambient lapse rate, set to $-6\,^{\circ}\mathrm{C\ km^{-1}}$. The cooling rate at ground surface is set to $-15\,\mathrm{W\,m^{-2}}$. Since we are most interested in calm night-time conditions, no wind in the domain is initially specified. The fixed pressure boundary condition (open boundary) is applied to lateral boundaries and top-boundary, where the pressure is close to 0.0 Pa, relative to the external pressure.

2.2 Conservation of mass and momentum

The flow is assumed to be steady and the Boussinesq approximation is applied. The mass, momentum, and energy balance equations in the canopy sub-layer can be writ-

ACPD
14, 28483–28522, 2014

ten as:

$$\frac{\partial \overline{u}_j}{\partial x_i} = 0 \tag{2}$$

$$\overline{u}_j \frac{\partial \overline{u}_i}{\partial x_j} = -\frac{1}{\rho}\frac{\partial P_*}{\partial x_i} + \nu \frac{\partial^2 \overline{u}_i}{\partial x_i x_j} - \frac{\partial}{\partial x_j}\left(\overline{u'_i u'_j}\right) - g_i \beta \left(\overline{\theta} - \theta_\infty\right) - F_{\mathrm{Di}} \tag{3}$$

$$\overline{u}_j \frac{\partial \overline{\theta}}{\partial x_j} = \Gamma \frac{\partial^2 \overline{\theta}}{\partial x_i x_j} - \frac{\partial}{\partial x_j}\left(\overline{\theta' u'_j}\right) + \frac{1}{\rho c_p} Q_{\mathrm{source}} \tag{4}$$

where $\overline{u}_i$ and $\overline{u}_j$ are the mean velocity components along x_i and x_j direction, respectively, $\overline{\theta}$ is the mean potential temperature, u'_i, u'_j and θ' are the fluctuations from their mean value $\overline{u}_i$, $\overline{u}_j$ and $\overline{\theta}$, ρ is the air density, ν is kinematic viscosity of air, P_* is the deviation of pressure from its reference value, β is the thermal expansion coefficient of air, and θ_∞ is the reference temperature, g_i is the gravity acceleration in i direction, $\Gamma = \nu/Pr$ is thermal diffusion coefficient, turbulent Prandtl number Pr is 0.5 in canopy layer and 1 above the canopy. $Pr = 0.5$ is close to the values used in large-eddy simulations of stably stratified atmospheric boundary layer turbulence (Basu and Porté-Agel, 2006; Stoll and Porté-Agel, 2008). In most of the region above the canopy (except very near the top of canopy), turbulence is very weak. In this region, molecular effects are dominant, especially in conditions without synoptic wind. Q_{source} is the energy source. When the atmosphere is stably stratified, $Q_{\mathrm{source}} < 0$ indicating radiative cooling of the canopy elements and ground surface. The constant cooling rate at the surface can drive a steady state stable boundary layer on flat and sloped terrain (Brost and Wyngaard, 1978), so we set $Q_{\mathrm{source}} = 0$ in the lower canopy layer (0–8 m) and then linearly decreased to $-8\,\mathrm{W\,m^{-3}}$ at the top canopy layer.

The steady state assumption is satisfied with condition proposed by Mahrt (1982),

$$F\hat{H}/\hat{T} \ll 1 \tag{5}$$

ACPD
14, 28483–28522, 2014

where F is the Froude number, $\hat{H}$ is the ratio of the average flow depth H to the surface elevation drop ΔZ_s, and $\hat{T}$ is the ratio of the time scale T to the Lagrangian time L/U. The Froude number is defined as

$$F = U^2 / \left(g \frac{\Delta\theta}{\theta_0} H \right) \tag{6}$$

where U is downslope velocity scale ($= O(10^{-1})\,\mathrm{m\,s^{-1}}$), g is gravity acceleration ($= 9.81\,\mathrm{m\,s^{-2}}$), $\Delta\theta$ is scale value for potential temperature deficit of the canopy layer ($= O(10^0)\,\mathrm{K}$), θ_0 is the basic state potential temperature ($= O(10^2)\,\mathrm{K}$), H is the flow depth scale, chosen to be the depth of significant temperature deficit which coincides with the layer of enhanced thermal stratification ($= O(10^1)\,\mathrm{m}$). In this simulation setting, $F = O(10^{-2})$. $\hat{H} = H/\Delta Z_s$, where $\Delta Z_s = L \sin\alpha$, L is downslope length scale ($= O(10^1)\,\mathrm{m}$), $\sin\alpha(\%) = O(10^1)$. Thus, $\hat{H} = O(10^0)$. $\hat{T} = TU/L$, where $T = O(10^4)\,\mathrm{s}$ is suggested by Mahrt (1982) to represent the order of magnitude of temporal accelerations associated with the diurnal evolution of drainage circulations. In our simulation, $\hat{T} = O(10^2)$. Thus, $F\hat{H}/\hat{T} = O(10^{-4}) \ll 1$.

F_{Di} is the drag force exerted by the canopy elements in i direction,

$$F_{Di} = \frac{1}{2} K_r u_i |U| \tag{7}$$

where K_r is the resistance coefficient, which is derived from an empirical relationship given by Hoener (1965),

$$K_r = \frac{1}{2}\left[\frac{3}{2\phi} - 1\right]^2 \tag{8}$$

where ϕ is porosity of the canopy layer, which can be obtained from leaf area density profile $a(z)$ (Gross, 1993),

$$\phi(z) = \frac{\sqrt{1 + 4a(z)} - 1}{2a(z)} \tag{9}$$

ACPD
14, 28483–28522, 2014

F_{Di} is zero above the canopy.

2.3 RNG k-ε model

The RNG model was developed by Yakhot and Orszag (1986a; b; Yakhot et al., 1992) using Re-Normalization Group (RNG) methods. The RNG k-ε turbulent model has been successfully applied in reproducing topographic and canopy related flows (Kim and Patel, 2000; Xu and Yi, 2013).

In RNG k-ε model, the Reynolds stress in Eq. (3) and turbulent heat flux in Eq. (4), respectively, are solved by turbulent viscosity, as:

$$-\overline{u_i' u_j'} = \mu_t \left(\frac{\partial \overline{u}_i}{\partial x_j} + \frac{\partial \overline{u}_j}{\partial x_i} \right) - \frac{2}{3} \delta_{ij} k \tag{10}$$

$$-\overline{\theta' u_j'} = \mu_\theta \frac{\partial \overline{\theta}}{\partial x_j} \tag{11}$$

where μ_t and $\mu_\theta = \mu_t / Pr$ are the turbulent viscosities of momentum and heat, respectively, δ_{ij} is Kronecker delta, and k is the turbulent kinetic energy.

RNG k-ε model assumes that turbulence viscosity in Eq. (10) is related to turbulence kinetic energy k (TKE) and dissipation ε:

$$\mu_t = \rho C_\mu \frac{k^2}{\varepsilon} \tag{12}$$

where k and ε are determined from the transport equations for k and ε; C_μ is a dimensionless constant.

ACPD
14, 28483–28522, 2014

The transport equations for k and its dissipation ε are written as:

$$\frac{\partial(k)}{\partial t} + \overline{u}_i \frac{\partial k}{\partial x_i} = \frac{\partial}{\partial x_i}\left(\frac{\mu_t}{\sigma_k}\frac{\partial k}{\partial x_i}\right) + P_\mathrm{s} + P_\mathrm{b} + P_\mathrm{w} + T_\mathrm{p} - \varepsilon \tag{13}$$

$$\frac{\partial(\varepsilon)}{\partial t} + \overline{u}_i \frac{\partial \varepsilon}{\partial x_i} = \frac{\partial}{\partial x_i}\left(\frac{\mu_t}{\sigma_\varepsilon}\frac{\partial \varepsilon}{\partial x_i}\right) + C_{\varepsilon 1}\frac{\varepsilon}{k}P_\mathrm{s} - \rho C_{\varepsilon 2}\frac{\varepsilon^2}{k} - S \tag{14}$$

where P_s is shear production, given by:

$$P_\mathrm{s} = \mu_t \frac{\partial \overline{u}_i}{\partial x_j}\left(\frac{\partial \overline{u}_i}{\partial x_j} + \frac{\partial \overline{u}_j}{\partial x_i}\right) \tag{15}$$

P_b is buoyancy production, given by:

$$P_\mathrm{b} = -\mu_\theta g_i \beta \frac{\partial \overline{\theta}}{\partial x_i} \tag{16}$$

P_w is wake production caused by canopy elements as (Meyers and Baldocchi, 1991):

$$P_\mathrm{w} = \overline{u}_i F_{\mathrm{D}i} = \frac{1}{2} K_\mathrm{r} |U| \overline{u}_i^2 \tag{17}$$

T_p is pressure collection term, which is calculated as residual of other TKE components, S is a volumetric source term which includes the rate-of-strain, given by:

$$S = \frac{C_\eta \eta^3 \left(1 - \frac{\eta}{\eta_0}\right)\varepsilon^2}{\left(1 + \beta_0 \eta^3\right) k} \tag{18}$$

$$\eta = \frac{k}{\varepsilon}\left[\frac{P_\mathrm{s}}{\mu_t}\right]^{1/2} \tag{19}$$

where the empirical constants C_μ, σ_k, σ_ε, $C_{\varepsilon 1}$, $C_{\varepsilon 2}$, β_0, and η_0 are 0.0845, 0.7194, 0.7194, 1.42, 1.68, 0.012, and 4.38, respectively (Yakhot and Orszag, 1986a; b).

ACPD
14, 28483–28522, 2014

3 Results and discussion

After a quasi-equilibrium condition is approached, all the solved fields in the studied cases are developed to be near symmetric horizontally (in the x-direction) with respect to the center of the modeled hill at $x = 0$ due to the homogeneous boundary conditions and initial settings. We restrict our discussion to the right half of the hill. Our results show (Fig. 1) that wind structure is differentiated into down-sweep ($H/L \leq 0.6$) and up-draft ($H/L \geq 0.8$) within canopy. The temperature, wind and turbulence characteristics on representative gentle ($H/L = 0.6$) and steep ($H/L = 1.0$) hills are illustrated (see Fig. 1) to explore the thermal and mechanical processes that govern the airflow structures.

3.1 Thermal analysis

In the model, strong stratification develops with distinct thermal distribution on the slope, subject to heat loss on the slope surface and the upper canopy layer. The heterogeneous distribution of heat within the canopy causes a "fish-head"-shaped temperature distribution on the slope, with the upper jaw in the upper canopy layer and the lower jaw attaching to the slope surface. The jaws consist of cold air while the open mouth shows relatively warmer air (Fig. 2). In comparison with the upper jaw which is confined to the middle and lower slope, the lower jaw extends up to the crest of the hill. As the slope intensity is reduced, the fish-head effect's upper jaw is diminished. For a very gentle slope (i.e., $H/L \ll 1$), the model produces a horizontal isotherm pattern with cold air at the bottom of the slope and warm air upslope, as would be expected in real-world conditions. A significant difference in temperature distribution among varied slopes results in a different angle of orientation of the fish-head temperature profile. Isotherms are inclined parallel to the slope surface because they tend to follow the shape of the slope and the top-canopy layer since the cooling along the slope surface is uniform. The temperature distribution on a gentle hill is shown as an angled fish-head shape, while the fish-head is tilted by the slope on the steep hill, which is shown

ACPD
14, 28483–28522, 2014

by the isotherms on the lower jaws. The different fish-head profile's angle can explain specific flow structures in the canopy (see Sect. 3.2). In accordance with the fish-head temperature distribution, temperature profiles are shown in three layers (Fig. 3a–d). A strong inversion layer is developed across the lower jaw, above which temperature slightly decreases with height in a thermal transition zone and a weak inversion layer is formed across the upper jaw. The temperature gradient and the depth of the lower inversion layer increases, since cold air flowing down the slope results in a cool pool on the lower slope where a single inversion layer extends above the canopy (Fig. 3e and f). The temperature difference from the hill surface to the top of the canopy at the hill crest is about 0.8 °C and 0.4 °C for gentle and steep hills, respectively, while the difference increases to around 3.2 °C in the canopy layer at the feet of both hills. The inversion strength near the surface is larger than in the upper canopy, which is due to the stronger radiative cooling effect on the surface. The temperature gradient and inversion on the steep hill are predicted weaker than on the gentle hill, because at the same horizontal x/L location, the canopy layer is at a higher elevation on the steep hill. Regardless of the horizontal location x/L, we find that inversions both near the surface and in the upper canopy are stronger on the steep hill than on the gentle hill at the same elevation, which benefits the development of stronger drainage flow on the steep slope.

Richardson number (Ri) is the ratio of the relative importance of buoyant suppression to shear production of turbulence, which is used to indicate dynamic stability and formation of turbulence. Ri is calculated based on mean profiles of wind and temperature. For different purposes and data availability, gradient Richardson number (Ri_g) and bulk Richardson number (Ri_b) are used to predict the stability within canopy. Yi et al. (2005) found that the gradient Richardson number,

$$Ri_g = \frac{\left(g/\overline{\theta}\right)\left(\partial\overline{\theta}/\partial z\right)}{\left(\partial\overline{U}/\partial z\right)^2} \quad (20)$$

ACPD
14, 28483–28522, 2014

With $\partial\overline{U}/\partial z = 0$ and $\partial\overline{\theta}/\partial z \neq 0$ at the inflection points of the S-shaped wind profile resulted in an infinite Ri_g, which describes the super-stable layer. In a forest, wind and temperature are typically only measured in a few levels, making $\partial\overline{U}/\partial z$ and $\partial\overline{\theta}/\partial z$ impossible to directly calculate. Therefore, Ri_b is commonly used to quantify stability between two levels (z_1 and z_2) using the measured temperature and wind speed (Zhang et al., 2010; Burns et al., 2011; Alekseychik et al., 2013),

$$Ri_b = \frac{g}{\overline{\theta}} \frac{\theta(z_2) - \theta(z_1)}{[U(z_2) - U(z_1)]^2} (z_2 - z_1) \tag{21}$$

In our modeling setting, the gridding space in vertical is $\Delta z = z_2 - z_1$, which is 0.5 m in the canopy layer. We define a local Richardson number to evaluate stability around the forested hill and examine the local stability in response to the heterogeneous distribution of heat. The local Richardson number in grid (m, n) is calculated as,

$$Ri_l = \frac{g}{\theta_{m,n}} \frac{\left(\theta_{m,n} - \theta_{m,n-1}\right)\left(z_{m,n} - z_{m,n-1}\right)}{\left(u_{m,n} - u_{m,n-1}\right)^2 + \left(w_{m,n} - w_{m,n-1}\right)^2} \tag{22}$$

Local Richardson number indicates that, within the canopy, flow is stably stratified except for an unstable region penetrating from the hill summit into the middle slope within the thermal transition regime (Fig. 1). Ri_l is found to be extremely large ($\sim 10^5$) just above the canopy on the upper to middle slope (Fig. 4a–d) indicating a thin primary super stable layer just above the top of canopy. The primary super stable layer is elevated and deepened on the lower slope (Fig. 4e and f), extended from the height of 1.3–1.4h to about the height of 2h. The deep primary super stable layer is caused by the strong cooling and temperature inversion at the base of the hill, regardless of slope intensity. Within canopy, a secondary super stable layer with extremely high Ri_l is developed below 0.5h. On the lower slope, the depth of the secondary super stable layer extends from the slope surface up to 0.5h due to strong temperature inversion and wind

ACPD
14, 28483–28522, 2014

stagnation. The absence of a secondary super stable layer on the summit could be explained by stronger entrainment of warmer air from above-canopy. Air in the transition region with negative temperature gradient is unstably stratified. The transition region is developed by the downwelling of cool air from the upper canopy with relatively warmer air upwelling from the lower canopy. The results show that for a sufficiently steep slope, the effects of the hill dominate the atmospheric profile, while for more gentle slopes the effects of the canopy dominates the resultant atmospheric profile.

The nocturnal stable canopy layer could be used to clarify the occurrence of within- and above- canopy flows decoupling observed in prior studies. Gorsel et al. (2011) reported a very stable nighttime canopy layer ($Ri_b > 1$) using the bulk Richardson number, indicating that the canopy layer is decoupled from air aloft. Decoupling at the top of the canopy is more likely to occur as the buoyancy is more dominant and air at the top of the canopy is strongly stable. The canopy top decoupling weakens vertical exchange of mass and heat between the vegetation and the atmosphere aloft. The measurement data show large temperature and CO_2 gradients (Burns et al., 2011) as decoupling occur in strongly stabilized atmosphere. Decoupling at the top of the canopy produced stronger carbon dioxide and temperature gradients than within canopy decoupling (Alekseychik et al., 2013). The primary super stable layer in our study is shown as a lid located at the top and above canopy, which could terminate the vertical exchange between the canopy and the air above. During nighttime, soil respiration contributes about 60–70 % (Janssens et al., 2001) of the total CO_2 emission from terrestrial ecosystem. The soil respired CO_2 could be blocked by the secondary super stable layer forming a very shallow pool on the slope surface.

3.2 Wind flow structures

Figure 1 shows that air above the canopy sinks and converges towards the hill and undergoes direction shift within canopy. Flow converges to the hill from all sides, and is then inflected near the top of the canopy, following the shape of the slope as drainage flow within the canopy. The height of inflection points increases as the air flows down

ACPD
14, 28483–28522, 2014

the slope. The inflection points are approximately at the bottom of the primary super stable layer. As a result of the abrupt convergence above the top of the canopy at the base of the hill, wake vortices are developed near the forest edge, after the wind leaves the hillside within the primary super stable layer. The wake vortices can extend to about 2.6L in horizontal and 1.3h in vertical. According to the flowing location within the canopy, we identify the drainage flow as two streams: the majority air mass within the upper-canopy inversion layer is called the upper-canopy drainage flow (UDF) layer; and the majority air mass within the inversion layer in the lower-canopy is called the lower-canopy drainage flow (LDF) layer. The UDF is developed as the air above the canopy sinks from the lateral sides towards the hill. However, the sinking motion is diverted following the shape of the top-canopy layer as it reaches the top of the canopy (Fig. 1). The UDF accelerates down the slope between the top of the unstable layer and the bottom of the primary super stable layer, reaching its maximum wind speed of 0.25 $\mathrm{m\,s^{-1}}$ at location (Fig. 5d) on the gentle slope and 0.35 $\mathrm{m\,s^{-1}}$ at location (Fig. 5e) on the steep slope, and then decelerates down to the feet of the hills. The air sinking over the crest can directly reach the surface of the crest and flow along the slope to form the LDF. The maximum wind speed of the LDF is at location (Fig. 5d) for a gentle slope (0.18 $\mathrm{m\,s^{-1}}$) and at location (Fig. 5c) for a steep slope (0.29 $\mathrm{m\,s^{-1}}$). The maximum wind speed in LDF occurs on the slope surface, below the secondary super stable layer. Deceleration of the flow towards the base of the hill should occur for a number of reasons. The pool of cool, dense air at the base of the hill resists incoming flow. Also, the drag force acting against the wind is dependent on the speed of the air flow squared.

UDF and LDF show different patterns within canopy for different slopes, which essentially determines the shift direction within canopy (Fig. 1). On the gentle slope (H/L = 0.6), UDF is much thicker compared with LDF. Air in UDF accelerates within the regime of the upper inversion layer reaching its maximum at the top of thermal transition region and then decelerates to a minimum (u = 0 and w = 0, Fig. 5) at the top of the slope surface inversion layer. Then, UDF sweeps horizontally to join the shallow LDF

ACPD
14, 28483–28522, 2014

on the slope surface, which is shown as negative streamwise velocity and near-zero vertical velocity in Fig. 5 (down-sweep). When the slope is steep (H/L = 1.0), UDF is much shallower than LDF. Air in LDF accelerates on the upper slope (Fig. 5a–c), followed by deceleration and stagnation. The stagnated flow jumps perpendicularly from deep canopy layer to join the shallow UDF in the upper canopy layer (The up-draft, with $u > 0$ and $w > 0$, is visible in Fig. 1 and 5). The shifting winds on both gentle and steep slopes are parallel to the isotherms in the warm "fish mouth" region of the profile. Rotational vortices are formed below the shifting winds.

The generation and direction of the shifting-wind structure are primarily driven by the slope and stratification. Under calm and stably stratified conditions, the dominant driving force of sinking drainage flow on the slope is the hydrostatic buoyancy force which is given as: $F_{hs} = g(\Delta\theta/\theta_0)\sin\alpha$, where α is the slope angle, $\Delta\theta$ is the potential temperature difference between the ambient air and the colder slope flow, θ_0 is the ambient potential temperature. The drainage flow on both the gentle and steep slopes is initiated by the dominant F_{hs} as the air is calm and stably stratified (Froude number $\ll$ 1, Belcher et al., 2008). The magnitude of F_{hs} increases with slope angle α so that F_{hs} is much larger on a steep slope than a gentle slope, leading to a stronger sinking motion above the crest. The sinking air penetrates to the lower part of the canopy at the hilltop. Thus, the LDF layer is deeper than the layer of UDF for a steep slope. However, the sinking motion above the crest on the gentle slope is diverted to follow the shape of the slope in the upper canopy due to smaller F_{hs}, which is not strong enough to completely penetrate the canopy. As a result, UDF is deeper than the LDF on gentle slopes, in contrast to that on steep slopes. The heterogeneous cooling in the canopy layer causes two baroclinic zones consistent with the UDF and LDF: the upper canopy layer and slope surface layer. The strong baroclinicity on the steep slope surface causes the deep LDF wind to rotate counter-clockwise (i.e., turning upwards on the lower slope, perpendicular to the hill slope). However, the rotated wind is forced to shift down when hitting the top-canopy UDF. The wind at the baroclinic zone with

ACPD
14, 28483–28522, 2014

a deep UDF on a gentle slope rotates clockwise, but shifts downslope when hitting the layer of the LDF.

3.3 Turbulent fluxes of momentum and heat

Figure 6 shows profiles of shear stress $-\overline{u'w'}$. Shear stress is most significant in the region near the top of the canopy where wind impinges on the canopy resulting in strong wind shear. Another region of large shear stress is in the lower canopy. This is related to the wind shifts which lead to strong wind shear. Shear stress is small on the upper slope but increases down the slope. The maximum shear stress at the top of the canopy is located at the wake region (Fig. 6e and f), where the wake vortices are formed. Shear stress is positive above the canopy indicating the downward transfer of momentum that is different from the usually observed downward transport of momentum in the upper canopy. It could be explained by the strong stability above the top of canopy, because strong stability substantially reduces the downward transport of momentum (Mahrt et al., 2000). The momentum transfer is reversed to upward ($-\overline{u'w'} < 0$) when approaching the top of the canopy where airflow is diverted into canopy layer because of the UDF and shear-production of turbulence. Strong upward momentum transfer near the top of canopy on the lower slope is associated with the wake generation behind the hill. In the upper canopy at midslope and downslope, shear stress decays rapidly as z decreases, because of the momentum absorption by the dense crown. The upward momentum ($-\overline{u'w'} < 0$) in the lower canopy indicates momentum sources in the LDF on steep slope. The LDF was recognized as jet-like flow in lower canopy, which has important effects on momentum transfer within canopy (Mao et al., 2007). Upward momentum transport in the canopy is very common, occurring in stable atmospheric conditions (Zhang et al., 2010). The opposite sign in momentum transfer near the slope surface on steep and gentle slope can be explained by the strength of LDF on the slope.

The dominant positive turbulent heat flux, $-\overline{w'\theta'}$ indicates downward heat transfer above and within the canopy (Fig. 7). Heat transfer on the upper slope (Fig. 7a and b)

ACPD
14, 28483–28522, 2014

is weak because the temperature difference between the canopy and the atmosphere above is small. The downward heat transfer is much stronger on the lower slope, where the air is cooled as a "cool pool" with the greatest temperature gradient. Turbulent heat flux increases towards the top of the canopy indicating increasing downward heat transfer ($-\overline{w'\theta'} > 0$) but the downward heat transfer decreases in the upper canopy layer. The peak of turbulent heat flux near the top of the canopy is due to the strong radiative cooling in the upper canopy. Below that the near zero and slightly upward turbulent heat flux (Fig. 7) is due to near neutral and negative temperature gradient in the thermal transition zone. As a result of the strong cooling in the ground surface, there are significant downward heat flux transfers in the lower canopy.

3.4 Turbulent Kinetic Energy (TKE) budget

In steady state, the TKE budget Eq. (13) can be written as:

$$0 = T_a + T_t + T_p + P_s + P_b + P_w - \varepsilon \quad (23)$$

where T_a is the advection of TKE by the mean wind, T_t represents the turbulent transport of TKE, T_p represents the transport of TKE by pressure perturbation, P_s is the shear production of TKE, P_b is buoyancy production of TKE, P_w is wake production of TKE and ε is viscous dissipation of TKE. We calculate all the terms in the TKE budget equation individually except T_p which is treated as the residual of other terms.

TKE is examined to show the intensity of turbulence along the slope (Fig. 8). TKE is usually low within the canopy implying a low turbulence flow under strongly stable atmospheric conditions. TKE is available near the top of canopy on the midslope and downslope. The region with strongly shifting winds is on the lower slope where the wind shear is strong. The largest TKE is found in the region of wake vortices across the canopy edge. The TKE value is larger on the gentle slope than on the steep slope.

Contributions from transport and production terms of TKE are complicated. P_b is a principal sink of TKE under stable conditions (Figs. 9 and 10). P_b exhibits negative values near the top of the canopy and slope surface, where flow is stably stratified, which

ACPD
14, 28483–28522, 2014

suppresses the turbulence around the top of the canopy and within the deep canopy. In the thermal transition zone, the contribution of P_b is minimal ($P_b \approx 0$ or slightly positive). Buoyancy production is neglected in some studies because P_b is (1) unimportant compared with other terms in TKE budget (Lesnik, 1974) and (2) difficult to measure (Meyers and Baldocchi, 1991), restricting the modeling and measurement studies to near-neutral conditions. Shen et al. (1997) showed that near the top of the canopy, the buoyancy production increases as instability increases, although it is smaller than 10 % of shear production in unstable conditions. Leclerc et al. (1990) illustrated a strong positive correlation between buoyancy production and stability ($P_b < 0$) or instability ($P_b > 0$) both within and above the canopy, which is confirmed in our modeling results.

Wake production (P_w) is a principal source of TKE in the upper half of the canopy where the canopy is dense (i.e., for large values of a and K_r) on both steep and gentle slopes. Although the magnitude of P_w is very small on a steep slope, the relative contribution of P_w is very large in comparison with other TKE components. Even in the lower canopy layer on the upper slope, P_w is a dominant source of TKE. This unusual phenomenon is induced by the deeper and stronger drainage flow on the slope surface.

The positive shear production P_s indicates the net transfer of kinetic energy from the mean flow to the turbulent component of the flow (Figs. 9 and 10). P_s is smaller than P_w except near the top of the canopy, which is consistent with the observations in soybeans (Meyers and Paw U, 1987), deciduous forests (Shi et al., 1987; Meyers and Baldocchi, 1991) and an artificial canopy (Raupach et al., 1987). P_s peaks at the top of the canopy, due to strong wind shear. Shear production is not as important as buoyancy and wake production in the canopy because of strong stability. Observational data also showed that shear production decreases with increasing stability in the lower two-thirds of the canopy (Leclerc et al., 1990).

Transport terms are the dominant source to maintain turbulent kinetic energy near the top of the canopy where strong buoyancy suppression occurs (Figs. 9 and 10). TKE is weakly transported by turbulence upward near the canopy top ($T_t < 0$) and downward ($T_t > 0$) in the canopy, because turbulence is limited by strong stability above the

ACPD
14, 28483–28522, 2014

canopy. TKE transport by advection and turbulence is unimportant at all levels and all slopes in comparison to pressure transport. The field measurement of pressure transport T_p is difficult and the behavior of T_p in the TKE budget is uncertain (Raupach et al., 1996; Finnigan, 2000). Maitani and Seo (1985), Shaw et al. (1990) and Shaw and Zhang (1992) have confirmed that T_p is not small enough to be neglected according to the surface pressure measurements. Pressure diffusion is recognized as an important sink of TKE in the upper canopy and source of TKE below (Dwyer et al., 1997) under unstable conditions. Our results show that the contribution of pressure transport to the overall TKE budget is significant when it is identified as a residual of other TKE components. T_p, which is of the same order as the production terms, supplies TKE in areas where the buoyancy suppression is very strong and extracts TKE where wake production is dominant. On gentle slopes, T_p is important to compensate the TKE loss by buoyancy near the top of the canopy and in the lower part of the canopy, and compensate TKE gain by wake motion in the upper half of the canopy (Fig. 9). On steep slopes, T_p on the lower half of the slope plays the same role as on gentle slopes to compensate the TKE loss by buoyancy and gain by wake (Fig. 10d–f), but the relative significance of wake production becomes more prominent. On the upper slope (Fig. 10a–c), pressure transport is important in the whole canopy to work against wake production. Our results suggest that the pressure perturbation is stronger compared with other terms on steep slopes. In addition, thermal effects on the upper steep slope are diminished and the canopy effect is magnified since the air is warm and the temperature gradient is small on the elevated topography.

4 Concluding remarks

The thermal stability and its influence on the canopy flow in complex terrain are explored in calm and stably stratified conditions. The thermal distribution and stability occurring within the canopy are substantially different from the ambient atmosphere. The stability around the canopy is characterized by stratification with a primary super

ACPD
14, 28483–28522, 2014

stable layer above the top of the canopy, a secondary super stable layer in the lower canopy, and an unstable layer within the canopy.

The thermal stratification around the canopy primarily drives the airflow and turbulent characteristics in the canopy layer on the slope. Airflow converges to the hill from all sides and the crest above the canopy, and is then inflected near the top of the canopy, following the shape of the slope, becoming drainage flow within the canopy. The drainage flow within the canopy is separated into two streams: the majority air mass in the upper canopy inversion layer is the upper-canopy drainage flow (UDF) layer; and the majority air mass in the inversion layer in the lower canopy is the lower-canopy drainage flow (LDF) layer. On gentle slopes, air in UDF sweeps horizontally to join the shallow LDF on the slope surface, while on steep slopes, the stagnated flow in LDF jumps upwards, perpendicular to the slope, from the lower canopy layer to join the shallow UDF in the upper canopy layer. The generation and direction of the shifting-wind structure within the canopy are induced by the hydrostatic buoyancy force and baroclinic instability on the slope, which are functions of the inclination of the slope.

The turbulent properties of the stratified canopy flow are closely associated with thermal and dynamic conditions on the slope. The downward transport of momentum in the canopy is reduced due to strong stability. Upward transport of momentum occurs in the deep canopy. The heat flux is predominantly transported downward with the minimum heat flux in the thermal transition zone in the middle of the canopy. TKE is available near the top of canopy on the midslope and downslope. The region experiencing strong wind shifts is on the lower slope where the wind shear is strong. The largest TKE values are found in the region of wake vortices across the canopy edge. Buoyancy production of TKE is a principal sink of TKE under stable conditions, which suppresses turbulence significantly near the top of the canopy and in the deep canopy. TKE is generated by shear production near the top of the canopy and by wake production in the canopy. The transport of TKE by pressure perturbation, which is of the same order as the production terms, supplies TKE where the buoyancy suppression is very strong and extracts TKE

ACPD
14, 28483–28522, 2014

where wake production is dominant. Our results suggest that the relative importance of pressure perturbation is enlarged as the slope increases.

The turbulent behavior in our results is solved by the modified Navier–Stokes Eqs. (2)–(4) with additional strong nonlinear terms (e.g. Chen and Yi, 2012). The energy source term in the Eq. (4), imposing constant heat flux at the ground surface and linearly increasing cooling rate in the upper canopy layer, acts as a driving force for the turbulence, while the drag term in the Eq. (3) acts as a dissipative force. The steady-state turbulent patterns (Fig. 1) result from balance between the thermal driving force from ground surface and canopy upper layer, drag dissipative force from canopy elements, and buoyancy forcing (compressibility effect) from thermal stratification and topography effects. Due to the imposed persistent heat flux forcing at ground surface and canopy upper layer, the steady-state formation is dominated by the thermal forcing.

Our numerical simulations have examined canopy turbulence behavior at the ultra-short wave scale in the whole spectrum of atmospheric turbulence study, with emphasis on strong boundary effects, including persistent thermal forcing from ground and canopy elements, strong damping force from canopy drag elements, and buoyancy effects from temperature stratification and topographic character. No available field measurements can be used to test the numerical simulation results yet. However, the fundamental characteristics of nighttime canopy flow over complex terrain measured by a few multi-tower advection experiments can be addressed by this numerical simulation, such as: (1) unstable layer in the canopy (Jacob et al., 1992), (2) super-stable layer associated with flow decoupling in deep canopy and near the top of canopy (Alekseychik et al., 2013; Yi et al., 2005), (3) upward momentum transfer in canopy (Dupont et al., 2012; Zhang et al., 2010), and (4) large buoyancy suppression and weak shear production in strong stability (Leclerc et al., 1990). The canopy flow behavior presented in Fig. 1 is expected to be measurable directly by multiple eddy-flux towers that are equipped with multi-level micrometeorological instruments (Feigenwinter et al., 2010; Baldocchi, 2008).

ACPD
14, 28483–28522, 2014

Acknowledgements. This research was supported, in part, under National Science Foundation Grants ATM-0930015, CNS-0958379 and CNS-0855217, PSC-CUNY Research Awards (Enhanced) ENHC-42-64, and the City University of New York High Performance Computing Center.

References

Alekseychik, I. Mammarella, P., Launiainen, S., Rannik, Ü., and Vesala, T.: Evolution of the nocturnal decoupled layer in a pine forest canopy, Agr. Forest Meteorol., 174–175, 15–27, 2013.

Aubinet, M. and Feigenwinter, C.: Direct CO_2 advection measurements and the night flux problem, Agr. Forest Meteorol., 150, 651–654, 2010.

Aubinet, M., Heinesch, B., and Yernaux, M.: Horizontal and vertical CO_2 advection in a sloping forest, Bound.-Lay. Meteorol., 108, 397–417, 2003.

Baldocchi, D. D.: "Breathing" of the terrestrial biosphere: lessons learned from a global network of carbon dioxide flux measurement systems, Austral. J. Bot., 56, 1–26, 2008.

Baldocchi, D. D. and Meyers, T. P.: Turbulence structure in a deciduous forest, Bound.-Lay. Meteorol., 43, 345–364, 1998.

Basu, S. and Porté-Agel, F.: Large-eddy simulation of stably stratified atmospheric boundary layer turbulence. A scale dependent dynamic modeling approach, J. Atmos. Sci., 63, 2074–2091, 2006.

Basu, S., Porté-Agel, F., Foufoula-Georgiou, E.,Vinuesa, J. F., and Pahlow, M.: Revisiting the local scaling hypothesis in stably stratified atmospheric boundary-layer turbulence. An integration of field and laboratory measurements with large-eddy simulations, Bound.-Lay. Meteorol., 119, 473–500, 2006.

Belcher, S. E., Finnigan, J. J., and Harman, I. N.: Flows through forest canopies in complex terrain, Ecol. Appl., 18, 1436–1453, 2008.

Bergen, J. D.: Vertical profiles of wind speed in a pine stand, For. Sci., 17, 314–322, 1971.

Biswas, G. and Eswaram, V. (Eds.): Turbulent Flows: Fundamentals, Experiments and Modeling, Narosa, 256 pp., 2002.

Brost, R. A. and Wyngaard, J. C.: A model study of the stably stratified planetary boundary layer, J. Atmos. Sci., 35, 1427–1440, 1978.

ACPD
14, 28483–28522, 2014

Burns, S. P., Sun, J., Lenschow, D. H., Oncley, S. P., Stephens, B. B., Yi, C., Anderson, D. E., Hu, J., and Monson, R. K.: Atmospheric stability effects on wind fields and scalar mixing within and just above a subalpine forest in sloping terrain, Bound.-Lay. Meteorol., 138, 231–262, 2011.

Chen, H. and Yi, C.: Optimal control of katabatic flows within canopies, Q. J. Roy. Meteor. Soc., 138, 1676–1680, doi:10.1002/qj.1904, 2012.

Coceal, O., Thomas, T. G., Castro, I. P., and Belcher, S. E.: Mean flow and turbulence statistics over groups of urban-like cubical obstacles, Bound.-Lay. Meteorol., 121, 49–519, 2006.

Cruz, M. G., Alexander, M. E., and Walimoto, R. H.: Development and testing of models for predicting crown fire rate of spread in conifer forest stands, Can. J. For. Res., 35, 1626–1639, 2005.

Denmead, O. T. and Bradley, E. F.: Flux-gradient relationships in a forest canopy, in: The Forest-Atmosphere Interaction, edited by: Hutchison, B. A. and Hicks, B. B., D. Reidel, Dordrecht, 421–442, 1985.

Dupont, S., Brunet, Y., and Finnigan, J. J.: Large-eddy simulation of turbulent flow over a forested hill: validation and coherent structure identification, Q. J. Roy. Meteor. Soc., 134, 1911–1929, 2008.

Dupont, S., Gosselin, F., Py, C., De Langere, E., Hemon, P., and Brunet, Y.: Modeling waving crops using large-eddy simulation: comparison with experiments and a linear stability analysis, J. Fluid Mech., 652, 5–44, 2010.

Dwyer, M. J., Patton, E. G., and Shaw, R. H.: Turbulent kinetic energy budgets from a large-eddy simulation of airflow above and within a forest canopy, Bound.-Lay. Meteorol., 84, 23–43, 1997.

Edburg, S. L., Allwine, G., Lamb, B., Stock, D., Thistle, H., Peterson, H., and Strom, B.: A simple model to predict scalar dispersion within a successively thinned loblolly pine canopy, J. Appl. Meteorol. Clim., 49, 1913–1926, 2010.

Feigenwinter, C., Montagnani, L., and Aubinet, M.: Plot-scale vertical and horizontal transport of CO2 modified by a persistent slope wind system in and above an alpine forest, Agr. Forest Meteorol., 150, 665–673, 2010.

Finnigan, J. J.: Turbulence in plant canopies, Annu. Rev. Fluid Mech., 32, 519–571, 2000.

Fons, W. L.: Influence of forest cover on wind velocity, J. For., 38, 481–486, 1940.

Galperin, B. and Orszag, S. A.: Large Eddy Simulation of Complex Engineering and Geophysical Flows, Cambridge University Press, 622 pp., 1993.

ACPD
14, 28483–28522, 2014

Gorsel, E. V., Harman, I. N., Finnigan, J. J., and Leuning, R.: Decoupling of air flow above and in plant canopies and gravity waves affect micrometeorological estimates of net scalar exchange, Agr. Forest Meteorol., 151, 927–933, 2011.

Goulden, M. L., Daube, B. C., Fan, S., Sutton, D. J., Bazzaz, A., Munger, J. W., and Wofsy, S. C.: Physiological response of a black spruce forest to weather, J. Geophys. Res., 102, 28987–28996, 1997.

Graham, J. and Meneveau, C.: Modeling turbulent flow over fractal trees using renormalized numerical simulation: alternate formulations and numerical experiments, Phys. Fluids, 24, 125105, doi:10.1063/1.4772074, 2012.

Gross, G.: Numerical Simulation of Canopy Flows, edited by: Douglas, J. and Marcus, M., Springer, Berlin, 167 pp., 1993.

Hoerner, S. F.: Fluid Dynamic Drag: Practical Information on Aerodynamic Drag and Hydrodynamic Resistence, Midland Park, NJ, 1965.

Huang, J., Cassiani, M., and Albertson, J. D.: The effects of vegetation density on coherent turbulent structures within the canopy sublayer: a large-eddy simulation study, Bound.-Lay. Meteorol., 133, 253–275, 2009.

Janssens, I. A., Lankreijer, H., Matteucci, G., Kowalski, A. S., Buchmann, N., Epron, D., Pilegaard, K., Kutsch, W., Longdoz, B., Grünwald, T., Montagnani, L., Dore, S., Rebmann, C., Moors, E. J., Grelle, A., Rannik, Ü., Morgenstern, K., Oltchev, S., Clement, R., Gudmundsson, J., Minerbi, S., Berbigier, P., Ibrom, A., Moncrieff, J., Aubinet, M., Bernhofer, C., Jensen, N. O., Vesala, T., Granier, A., Schulze, E. D., Lindroth, A., Dolman, A. J., Jarvis, P. G., Ceulemans, R., and Valentini, R.: Productivity overshadows temperature in determining soil and ecosystem respiration across European forests, Glob. Change Biol., 7, 269–278, 2001.

Katul, G. G., Finnigan, J. J., Poggi, D., Leuning, R., and Belcher, S. E.: The influence of hilly terrain on canopy-atmospheric carbon dioxide exchange, Bound.-Lay. Meteorol., 118,189–216, 2006.

Kim, H. G. and Patel, V. C.: Test of turbulence models for wind flow over terrain with separation and recirculation, Bound.-Lay. Meteorol., 94, 5–21, 2000.

Lalic, B. and Mihailovic, D. T.: A new approach in parameterization of momentum transport inside and above forest canopy under neutral conditions, integrated assessment and decision support, in: Proceedings of the 1st Biennial Meeting of the International Environmental Modelling Software Society, Switzerland, iEMSs, Manno, 139–154, 24–27 June, 2002.

ACPD
14, 28483–28522, 2014

Landsberg, J. J. and James, G. B.: Wind profiles in plant canopies: studies on an analytical model, J. Appl. Ecol., 8, 729–741, 1971.
Leclerc, M. Y., Beissner, K. C., Shaw, R. H., den Hartog, G., and Neumann, H. H.: The influence of atmospheric stability on the budgets of the reynolds stress and turbulent kinetic energy within and above a deciduous forest, J. Appl. Meteorol., 29, 916–933, 1990.
Lemon, E., Allen, L. H., and Muller, L.: Carbon dioxide exchange of a tropical rain forest, BioScience, 20, 1054–1059, 1970.
Lesnik, G. E.: Results of measurement of turbulent energy balance components in a layer of vegetation, Izv. Atmos. Oceanic Phys., 10, 652–655, 1974.
Mahrt, L.: Momentum balance of gravity flows, J. Atmos. Sci., 39, 2701– 2711, 1982.
Mahrt, L., Lee, X., Black, A., Neumann, H., and Staebler, R. M.: Nocturnal mixing in a forest subcanopy, Agr. Forest Meteorol., 101, 67–78, 2000.
Maitani, T. and Seo, T.: Estimates of velocity-pressure and velocity-pressure gradient interactions in the surface layer over plant canopies, Bound.-Lay. Meteorol., 33, 51–60, 1985.
Mao, S., Feng, Z., and Michaelides, E. E.: Large-eddy simulation of low-level jet-like flow in a canopy, Environ. Fluid Mech., 7, 73–93, 2007.
Mao, S., Leclerc, M. Y., and Michaelides, E. E.: Passive scalar flux footprint analysis over horizontally inhomogenous plant canopy using large-eddy simulation, Atmos. Environ., 42, 5446–5458, 2008.
Meyers, T. P. and Baldocchi, D. D.: The budgets of turbulent kinetic energy and Reynolds stress within and above deciduous forest, Agr. Forest Meteorol., 53, 207–222, 1991.
Meyers, T. P. and Paw U, K. T.: Testing of a higher-order closure model for modeling airflow within and above plant canopies, Bound.-Lay. Meteorol., 37, 297–311, 1986.
Montagnani, L., Manca, G., Canepa, E., Georgieva, E., Acosta, M., Feigenwinter. C., Janous, D., Kerschbaumer, G., Lindroth, A., Minach, L., Minerbi, S., Mölder, M., Pavelka, M., Seufert, G., Zeri, M., and Ziegler, W.: A new mass conservation approach to the study of CO_2 advection in an alpine forest, J. Geophys. Res., 114, D07306, doi:10.1029/2008JD010650, 2009.
Oliver, H. R.: Wind profiles in and above a forest canopy, Q. J. Roy. Meteor. Soc., 97, 548, 1971.
Pinard, J. and Wilson, J. D.: First- and second-order closure models for wind in a plant canopy, J. Appl. Meteorol., 40, 1762–1768, 2001.

ACPD
14, 28483–28522, 2014

Poggi, D. and Katul, G. G.: The ejection-sweep cycle over gentle hills covered with bare and forested surfaces, Bound.-Lay. Meteorol., 122, 493–515, 2007.
Queck, R. and Bernhofer, C.: Constructing wind profiles in forests from limited measurements of wind and vegetation structure, Agr. Forest Meteorol., 150, 724–735, 2010.
Raupach, M. R.: A Lagrangian analysis of scalar transfer in vegetation canopies. Q. J. Roy. Meteor. Soc., 113, 107–130, 1987.
Raupach, M. R., Finnigan, J. J., and Brunet, Y.: Coherent eddies and turbulence in vegetation canopies: the mixing-layer analogy, Bound.-Lay. Meteorol., 78, 351–382, 1996.
Ross, A. N.: Large-eddy simulation of flow over forested ridges, Bound.-Lay. Meteorol., 128, 59–76, 2008.
Ross, A. N. and Vosper, S. B.: Neutral turbulent flow over forested ridges, Q. J. Roy. Meteor. Soc., 131, 1841–1862, 2005.
Schaeffer, S. M., Miller, J. B., Vaughn, B. H., White, J. W. C., and Bowling, D. R.: Long-term field performance of a tunable diode laser absorption spectrometer for analysis of carbon isotopes of CO_2 in forest air, Atmos. Chem. Phys., 8, 5263–5277, doi:10.5194/acp-8-5263-2008, 2008.
Schlichting, H.: Boundary Layer Theory, 4th edn., McGraw-Hill, New York, USA, 647 pp., 1960.
Shaw, R. H.: Secondary wind speed maxima inside plant canopies, J. Appl. Meteorol., 16, 514–521, 1977.
Shaw, R. H. and Zhang, X. J.: Evidence of pressure-forced flow in a forest, Bound.-Lay. Meteorol., 58, 47–64, 1992.
Shaw, R. H., Paw U, K. T., Zhang, X. J., Gao, W., Den Hartog, G., and Neumann, H. H.: Retrieval of turbulent pressure fluctuations at the ground surface beneath a forest, Bound.-Lay. Meteorol., 50, 319–338, 1990
Shi, G., Shaw, R. H., Thurtell, G. W., den Hartog, G., and Neumann, H. H.: The turbulent kinetic energy budget within and above a deciduous forest, in: 18th Conf. on Agric., and For. Meteor., 15–18 September 1987, W. Lafayette, Indiana, Amer. Meteor. Soc., Boston, 187–188, 1987.
Siebicke, L., Hunner, M., and Foken, T.: Aspects of CO_2 advection measurements, Theor. Appl. Climatol., 109, 109–131, 2012.
Smith, L. M. and Reynolds, W. C.: On the Yakhot-Orszag Renormalization group method for deriving turbulence statistics and models, Phys. Fluids A, 4, 364, 1992.
Staebler, R. M. and Fitzjarrald, D. R.: Observing subcanopy CO_2 advection, Agr. Forest Meteorol., 12, 139–156, 2004.

ACPD
14, 28483–28522, 2014

Stoll R. and Porté-Agel, F.: Large-eddy simulation of the stable atmospheric boundary layer using dynamic models with different averaging schemes, Bound.-Lay. Meteorol., 126, 1–28, 2008.

Sun, J., Burns, S. P., Delany, A. C., Oncley, S. P., Turnipseed, A. A., Stephens, B. B., Lenschow, D. H., LeMone, M. A., Monson, R. K., and Anderson, D. E.: CO_2 transport over complex terrain, Agr. Forest Meteorol., 145, 1–21, 2007.

Sypka, P. and Starzak, R.: Simplified, empirical model of wind speed profile under canopy of Istebna spruce stand in mountain valley, Agr. Forest Meteorol., 171–172, 220–233, 2013.

Tennekes, T. and Lumley, J. L.: A First Course in Turbulence, MIT, Cambridge, MA, 300 pp., 1972.

Tóta, J., Fitzjarrald, D. R., and da Silva Dias, M. A. F.: Amazon rainforest exchange of carbon and subcanopy air flow Manaus LBA site- a complex terrain condition, The Scientific World J., 2012, 165067, doi:10.1100/2012/165067, 2012.

Turnipseed, A. A., Anderson, D. E., Blanken, P. D., Baugh, W. M., and Monson, R. K.: Airflows and turbulent flux measurements in mountainous terrain Part 1. Canopy and local effects, Agr. Forest Meteorol., 119, 1–21, 2003.

von Kármán, Th.: Mechanische Ähnlichkeit und Turbulenz, Nachrichten von der Gesellschaft der Wissenschaften zu Göttingen, Fachgruppe 1 (Mathematik) 5, 58–76, 1930.

Wang, W.: The influence of topography on single-tower-based flux measurement under unstable condition: a modeling perspective, Theor. Appl. Climatol., 99, 125–138, 2010.

Wang, W. and Yi, C.: A new nonlinear analytical model for canopy flow over a forested hill, Theor. Appl. Climatol., 109, 549–563, 2012.

Wilson, J. D., Finnigan, J. J., and Raupach, M. R.: A first-order closure for disturbed plant-canopy flows, and its application to winds in a canopy on a ridge, Q. J. Roy. Meteor. Soc., 124, 705–732, 1998.

Wolfe, G. M., Thornton, J. A., McKay, M., and Goldstein, A. H.: Forest-atmosphere exchange of ozone: sensitivity to very reactive biogenic VOC emissions and implications for in-canopy photochemistry, Atmos. Chem. Phys., 11, 7875–7891, doi:10.5194/acp-11-7875-2011, 2011.

Xu, X. and Yi, C.: The influence of geometry on recirculation and CO_2 transport over forested hills, Meteorol. Atmos. Phys., 119, 187–196, 2013.

Yakhot, V. and Orszag, S. A.: Renormalization group analysis of turbulence: basic theory, J. Sci. Comput., 1, 3–61, 1986a.

ACPD
14, 28483–28522, 2014

Yakhot, V. and Orszag, S. A.: Renormalization group analysis of turbulence, Phys. Rev. Lett., 57, 1722–1724, 1986b.
Yakhot, V., Orszag, S. A., Thangam, S., Gatski, T. B., and Speziale, C. G.: Development of turbulence models for shear flows by a double expansion technique, Phys. Fluids A, 4, 1510–1520, 1992.
Yi, C.: Momentum transfer within canopies, J. Appl. Meteorol. Clim., 47, 262–275, 2008.
Yi, C., Monsoon, R. K., Zhai, Z., Anderson, D. E., Lamb, B., Allwine, G., Turnipseed, A. A., and Burns, S. P.: Modeling and measuring the nocturnal drainage flow in a high-elevation, subalpine forest with complex terrain, J. Geophys. Res., 110, D22303, doi:10.1029/2005JD006282, 2005.
Yi, C., Anderson, D. E., Turnipseed, A. A., Burns, S. P., Aparks, J. P., Stannard, D. I., and Monson, R. K.: The contribution of advective fluxes to net eecosystem exchange in a high-elevation, subalpine forest, Ecol. Appl., 18, 1379–1390, 2008.
Zhang, G., Leclerc, M. Y., and Karipot, A.: Local flux-profile relationships of wind speed and temperature in a canopy layer in atmospheric stable conditions, Biogeosciences, 7, 3625–3636, doi:10.5194/bg-7-3625-2010, 2010.

ACPD
14, 28483–28522, 2014

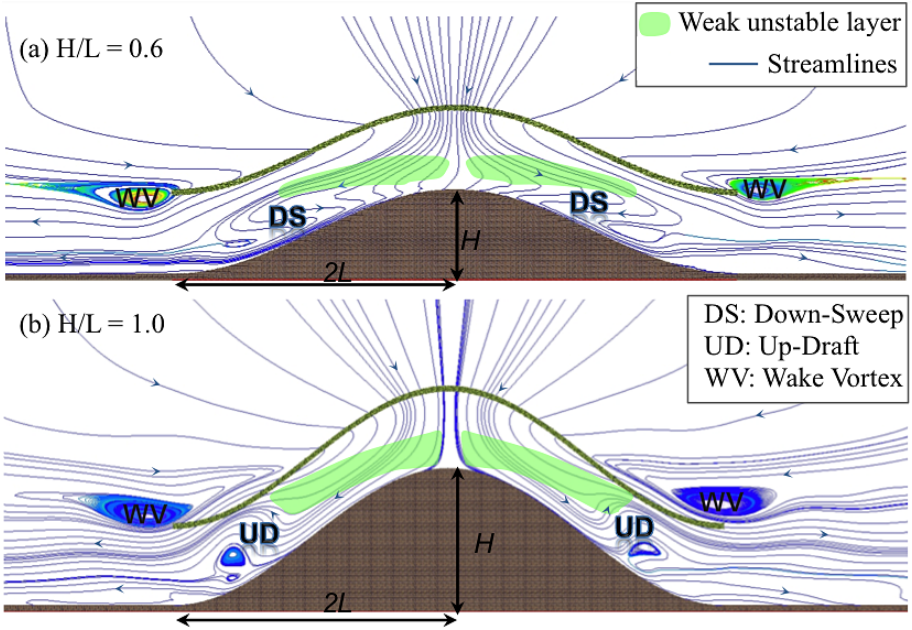

Figure 1. Simulated streamlines in the forested hill: **(a)** H/L = 0.6; **(b)** H/L = 1.0. The translucent green masks indicate the regimes with instability within canopy. The black "WV" marks the region of wake vortices next to the edge of canopy. The "DS" in **(a)** and "UD" in **(b)** indicate the region of down-sweep wind and up-draft wind on the gentle and steep slopes, respectively.

ACPD
14, 28483–28522, 2014

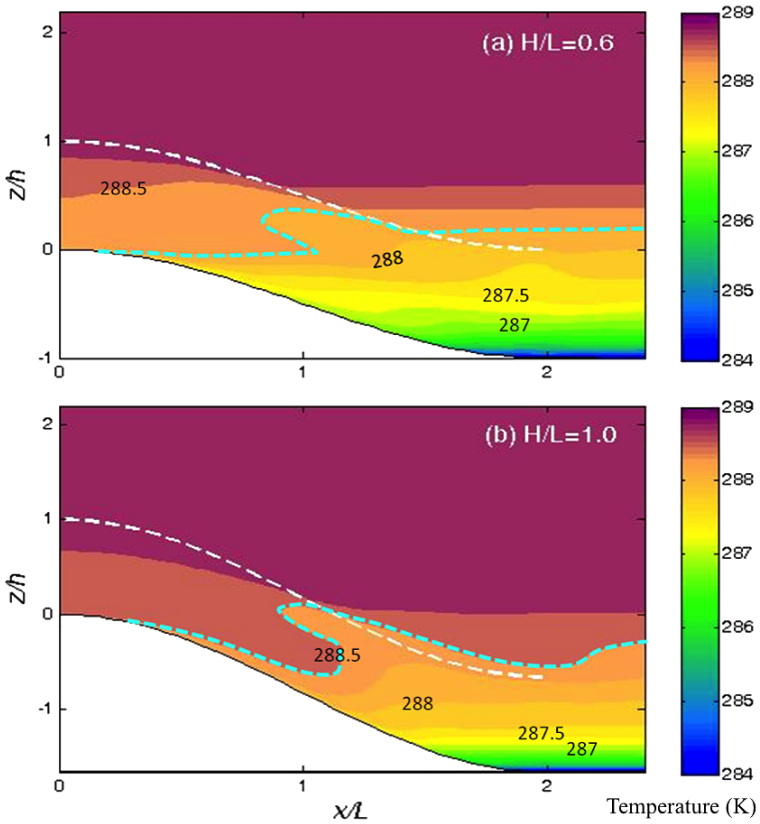

Figure 2. Contours of potential temperature (K) along the right slope: **(a)** $H/L = 0.6$; **(b)** $H/L = 1.0$. The difference between isotherms is 0.25 K. The numbers on isotherms indicate the temperature. The x axis is normalized by the half length scale of the hill L and y axis is normalized by the height of the canopy h. White dashed lines indicate the top of canopy and the isotherms marked with green dashed lines highlight the "fish-head" temperature distribution.

ACPD
14, 28483–28522, 2014

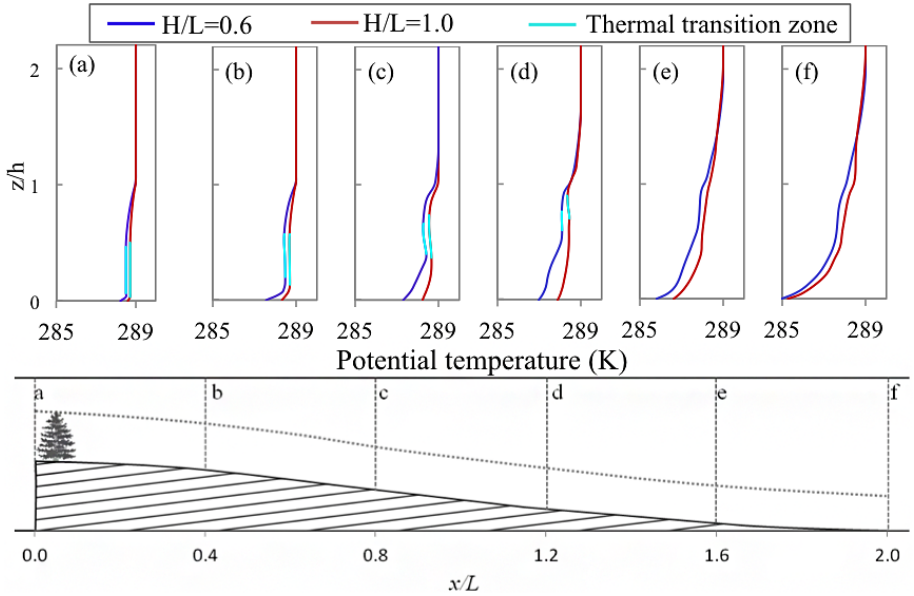

Figure 3. Potential temperature (K) profiles on the slope for $H/L = 0.6$ (blue) and $H/L = 1.0$ (red). The locations of the six sections are labeled as **(a–f)**, and their locations with respect to the hill are presented, which is normalized by the half length scale L. The green curves indicate the thermal transition zone with negative temperature gradient.

ACPD
14, 28483–28522, 2014

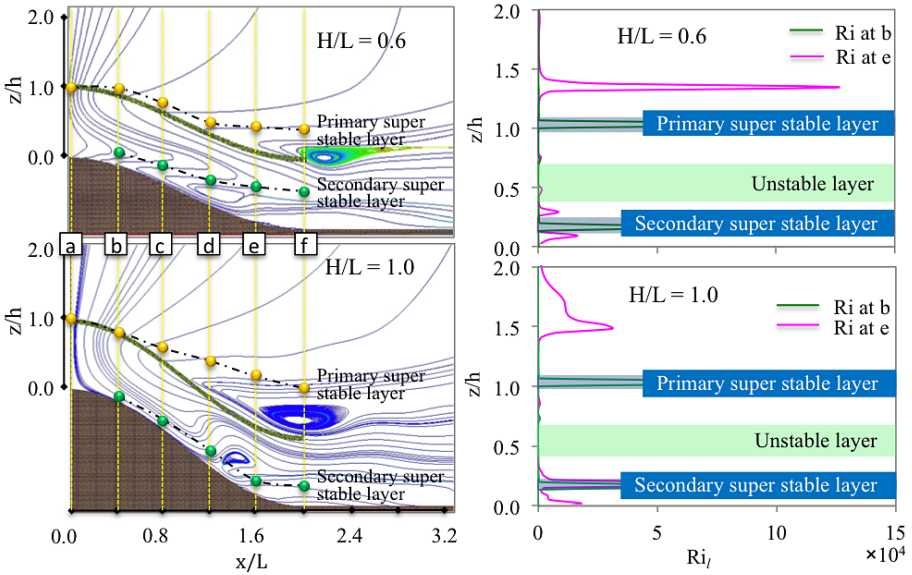

Figure 4. Locations of super stable layers for $H/L = 0.6$ and $H/L = 1.0$ (left panel). The primary super stable layers are marked by dash-dotted lines with yellow solid circles and secondary super stable layers are marked by dash-dotted lines with green solid circles. The *Ri* numbers at locations indicated by the yellow and green solid circles are extremely large, which are illustrated on the right panel for the locations b and e.

ACPD
14, 28483–28522, 2014

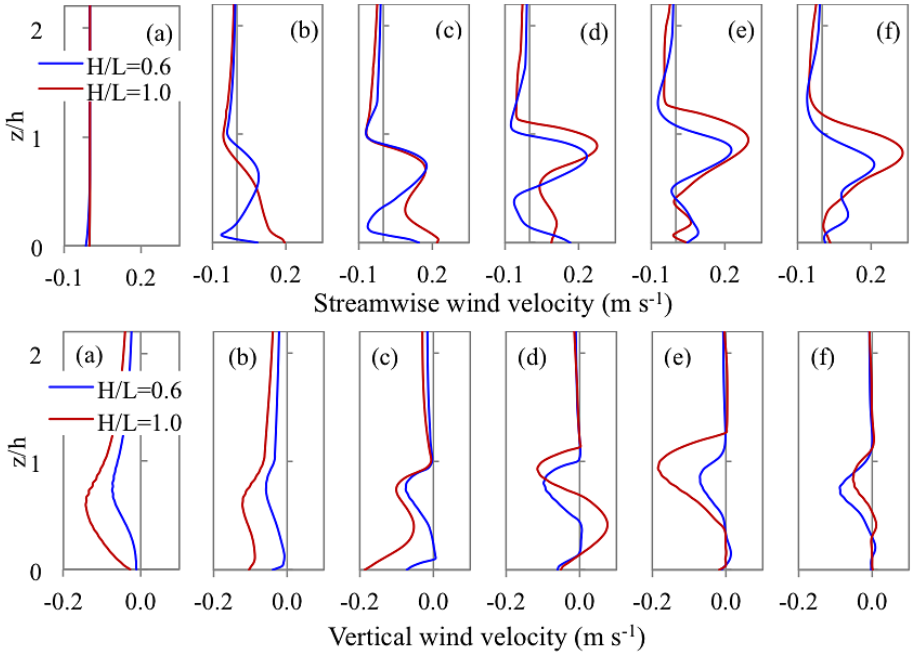

Figure 5. Profiles of streamwise velocity ($m\,s^{-1}$, top panel) and vertical velocity ($m\,s^{-1}$, bottom panel) for H/L = 0.6 (blue) and H/L = 1.0 (red). The locations of the six sections are labeled as **(a–f)**, and their locations with respect to the hill are presented in Fig. 3.

ACPD
14, 28483–28522, 2014

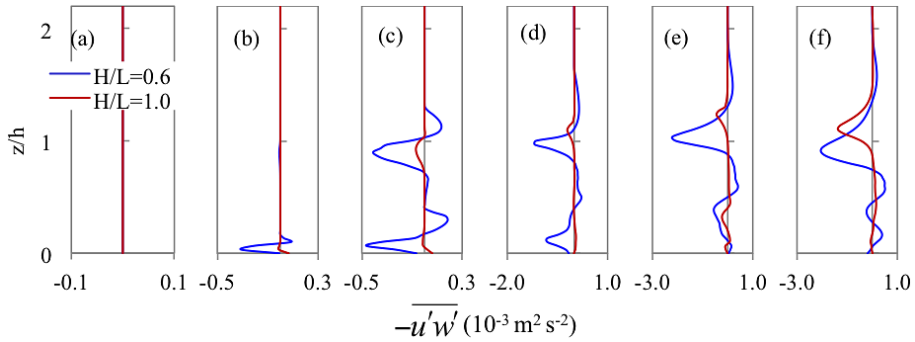

Figure 6. Profiles of shear stress, $-\overline{u'w'}$ ($10^{-3}\,m^2\,s^{-2}$) on the slope for $H/L = 0.6$ (blue) and $H/L = 1.0$ (red). The locations of the six sections are labeled as **(a–f)**, and their locations with respect to the hill are presented in Fig. 3.

ACPD
14, 28483–28522, 2014

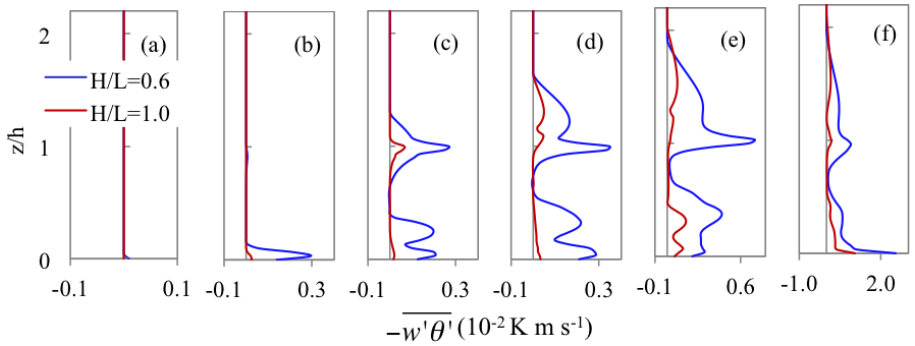

Figure 7. Profiles of turbulent Heat Flux, $-\overline{w'\theta'}$ (10^{-2} K m s^{-1}) on the slope for H/L = 0.6 (blue) and H/L = 1.0 (red). The locations of the six sections are labeled as **(a–f)**, and their locations with respect to the hill are presented in Fig. 3.

ACPD
14, 28483–28522, 2014

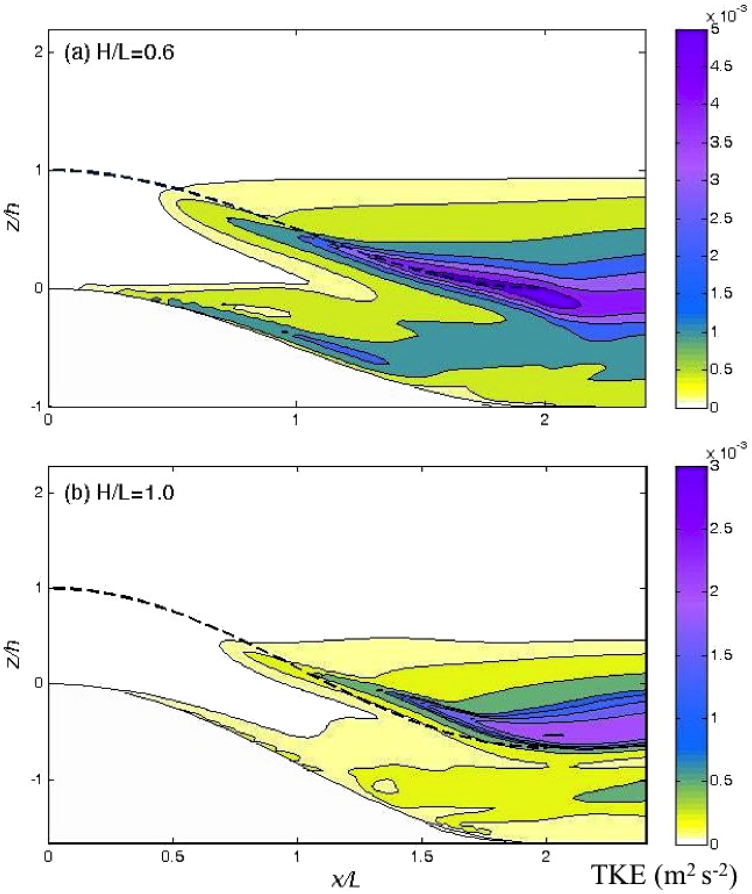

Figure 8. Contours of turbulent kinetic energy ($m^2\,s^{-2}$): **(a)** H/L = 0.6; **(b)** H/L = 1.0. The black dashed lines indicate the top of canopy.

ACPD
14, 28483–28522, 2014

Stably stratified canopy flow in complex terrain

X. Xu et al.

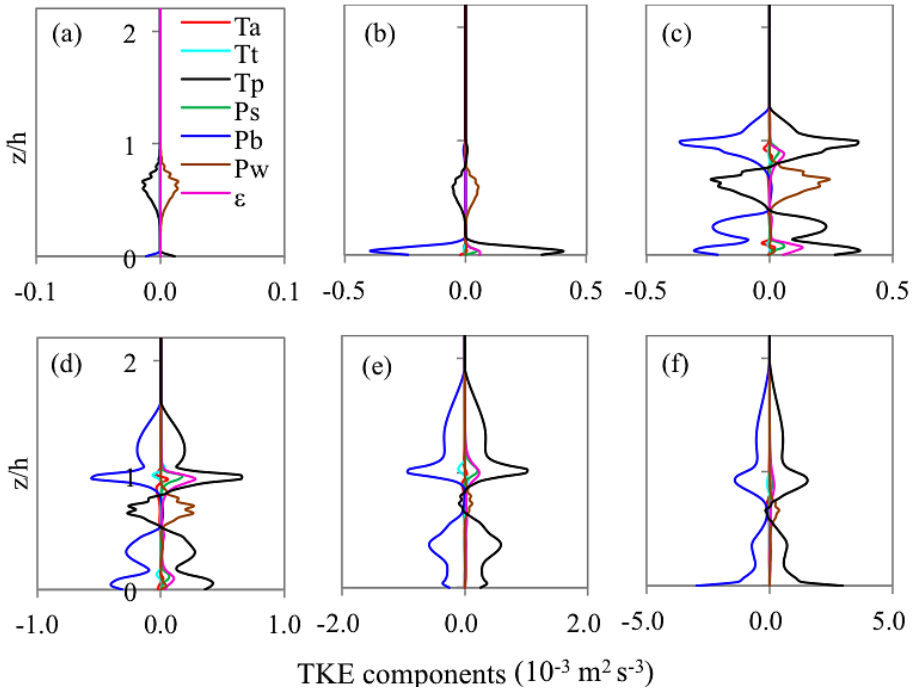

Figure 9. Profiles of TKE components (10^{-3} m^2 s^{-3}) for H/L = 0.6. T_a is the advection of TKE by the mean wind, T_t represents the turbulent transport of TKE, T_p represents the transport of TKE by pressure perturbation, P_s is the shear production of TKE, P_b is buoyancy production of TKE, P_w is wake production of TKE and ε is viscous dissipation of TKE. The locations of the six sections are labeled as **(a–f)**, and their locations with respect to the hill are presented in Fig. 3.

ACPD
14, 28483–28522, 2014

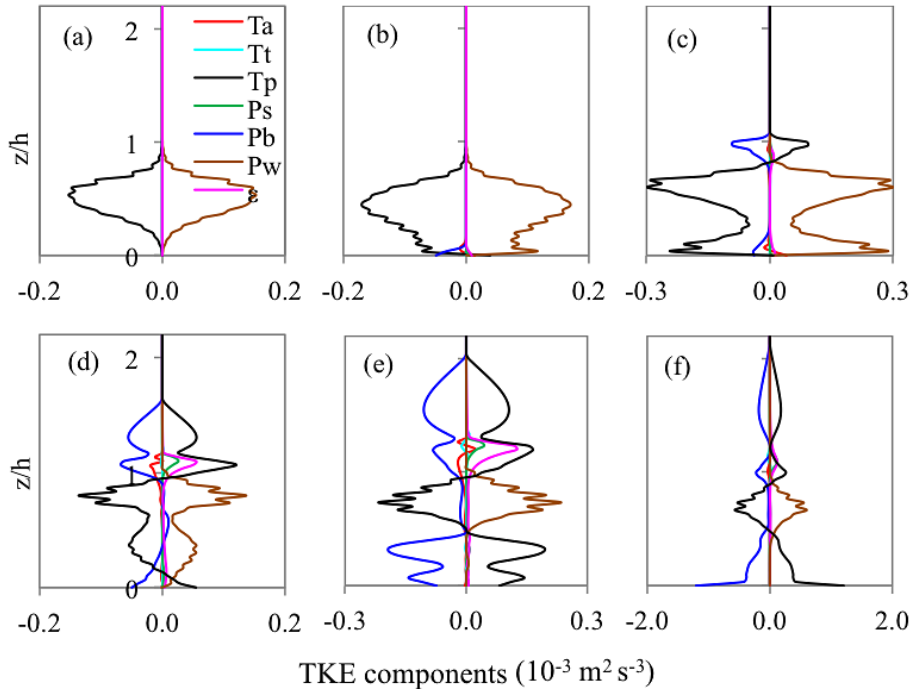

Figure 10. The same as in Fig. 9, but for H/L = 1.0.

ACPD
14, 28483–28522, 2014